Fabrication of Perovskite-type Oxide BaPbO₃ Nanoparticles and their Efficiency in Photodegradation of Methylene Blue

Taymaz Tabari[a,*] Haman Tavakkoli[b], Poorya Zargaran[a] and Davoud Beiknejad[a]

[a]*Department of Chemistry, Faculty of Sciences, Gorgan Branch, Islamic Azad University, Gorgan, Iran.*
[b]*Department of Chemistry, Science and Research Branch, Islamic Azad University, Khouzestan, Iran.*

ABSTRACT

BaPbO₃ perovskite was prepared by the sol-gel method. The physical and chemical properties of catalyst were characterized by XRD, TEM, SEM, EDX and IR techniques. The photocatalytic activity of the sample was evaluated by photocatalytic decomposition of methylene blue (MB) dye under UV irradiation. The results of XRD indicate that the perovskite-type oxide (BaPbO₃) is crystal at 700 °C. The XRD, TEM and SEM revealed that BaPbO₃ particles are prepared in the nano-size regime. The results show that the degradation efficiency of methylene blue (MB) by BaPbO₃ is higher than rutile under similar conditions.

KEYWORDS

Perovskite-type oxide, nanopowder, dye removal, methylene blue.

1. Introduction

Due to the increasing environmental pollution in recent years, the degradation of organic pollutants has generated a broader interest in photocatalysis for both scientific understanding and potential applications.[1,2] Some dyes and their degradation products, in surface water, are reported to be highly carcinogenic.[3] It is, therefore, essential to treat the dye effluents prior to their discharge into the receiving water. Dyes are organic compounds consisting of two main groups of compounds, chromophores (responsible for colour of the dye) and auxochromes (responsible for intensity of the colour).[4] Dyes are classified according to chemical structure and type of application. Based on the chromophore, 20–30 different groups of dyes can be discerned, with azo, anthraquinone, phthalocyanine and triarylmethane accounting for the most important groups. Azo (around 70 %) and anthraquinone (around 15 %) comprise the largest classes of dyes. Many processes are employed to remove dye molecules from coloured effluents. In general, treatment methods can be divided into three categories: (i) physical methods such as adsorption[5-7] and membrane filtration;[8] (ii) chemical methods such as ionic exchange,[9] chemical oxidation,[10,11] electrochemical degradation[12] and ozonation;[13] and (iii) biological degradation.[14] Adsorption techniques for wastewater treatment have become more popular in recent years because of their efficiency in the removal of pollutants which are stable in biological degradation processes. Adsorption can produce high quality water while also being a process that is economically feasible.[15] The physical characteristics of the adsorbents, such as surface area, porosity, size distribution, density and surface charge, all influence the adsorption process. As a result, there is interest in developing new adsorbent materials with diverse compositions, properties and functionalities. The family of perovskite-type oxides generally formulated as ABO₃ (A is a rare earth metal with large ionic radius or alkali earth metals; B is a transition metal with a small ionic radius) could be considered as an adsorbent/catalyst material for the removal of dyes.[16,17]

In our earlier experiment, we tested the LCNO perovskite-type nanoparticles as a novel adsorbent to remove of reactive blue 5 (RB5) dye.[18] This study investigated the efficiency of BaPbO₃, perovskite nanoparticles, as adsorbent for removal of the azo-dye, methylene blue (MB), (Fig. 1) from an aqueous solution. The effect of different variables including concentration of dye, pH, adsorbent doses and reaction time, were evaluated. Furthermore, preparation of BaPbO₃ nanoparticles *via* the sol-gel method and its characterization by different techniques such as IR, XRD, SEM-EDX and TEM is reported.

2. Experimental

2.1. Preparation of Catalyst

The sol-gel method was used to prepare BaPbO₃ nanoparticles; Barium carbonate and citric acid were dissolved in deionized water in the molar ratio 1:1 and the pH adjusted to 8 using aqueous ammonia. PbO was added to the solution heated to 50 °C with stirring. When the solvent was slowly evaporated, a homogeneous sol was formed. The sol was dried for 6 h at 80 °C in a dry box until it became a gel. The gel was calcined at 700 °C for 2 h with a slow heating rate (2 °C min⁻¹) and finally ground into a powder.

The complex polymeric gel and derived powders were analyzed by Fourier transform infrared (FTIR) spectroscopy on a thermo Nicollet Nexus 870 FTIR spectrometer. The crystallinity and microstructure of the oxide powders were characterized with an X-ray diffractometer employing a scanning rate of 0.02 S-1 in a 2θ range from 0 to 70 °, using a Philips X pert, 200, equipped with CuKα radiation. The data were analyzed using JCPDS standards.
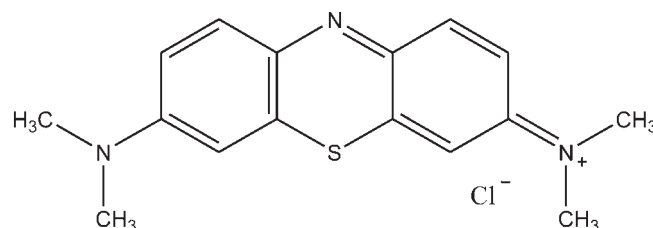

Figure 1 Chemical structure of methylene blue (MB).

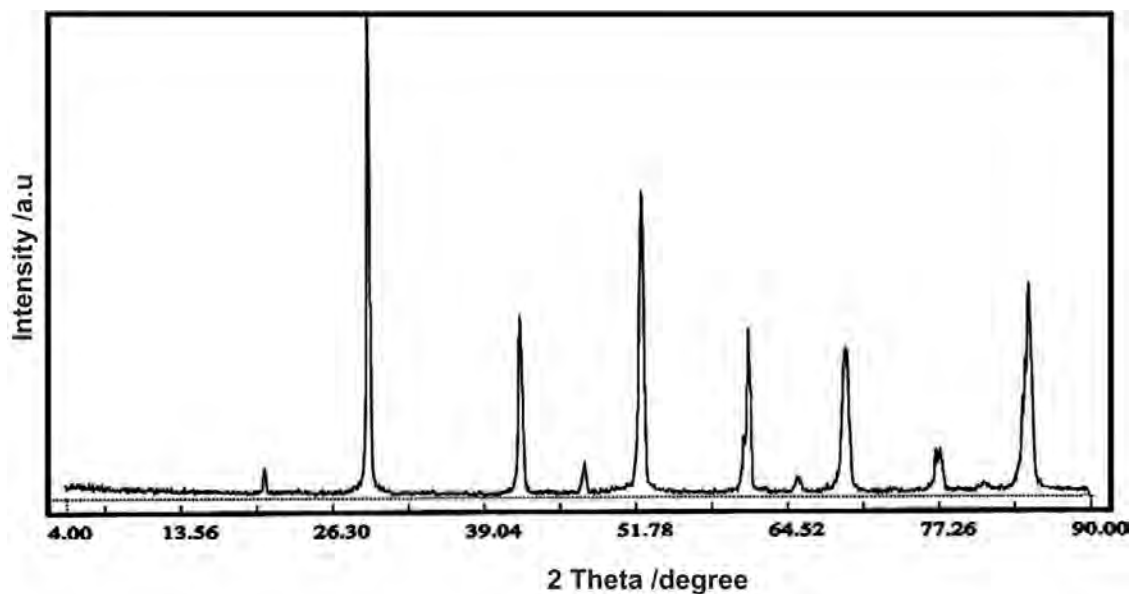*To whom correspondence should be addressed. E-mail: taymaz_tabari@yahoo.com

Figure 2   XRD pattern of BaPbO$_3$ nanoparticles calcined at 700 °C.

The microstructure of the nanoparticles was observed by transmission electron microscope (TEM) using a LEO 912AB microscope and an accelerating voltage of 120 kV. The morphology and chemical analysis of the particles was investigated using SEM-EDX. The SEM of the type LEO 1450 VP (V = 30 kV) was equipped with an EDX spectrometer of the type Inca 400 (Oxford Instruments).

2.2. Activity Test of Catalyst

Photocatalytic tests were carried out in a batch-type reactor with an inner irradiation cell. With vigorous stirring, 0.2 g of powdered BaPbO$_3$was dispersed in 100 mL of an aqueous solution containing 30 mg L^{-1} of MB. This dispersion was stirred for 1 h, in the dark, to establish the adsorption–desorption equilibrium. Immediately thereafter, the dispersion was irradiatedwith UV light. 5 mL aliquots were collected every 15 min for analysis. In all the tests, a source of monochromatic radiation ($\lambda = 254$ nm) with a power of 12 W was used. The photocatalytic activity was evaluated from the decrease of the MB concentration under UV irradiation. Moreover, the test of ultraviolet light absorption characteristics was performed using a JASCO, UV-550 type ultraviolet spectrophotometer.

3. Results and Discussion

3.1. X-ray Diffraction

Figure 2 shows the powder X-ray diffraction patterns of the sample prepared by the sol-gel method, the product exhibited sharp peaks indicating a high degree of crystallinity during calcination. XRD results reveal the existence of aperovskite-type phase BaPbO$_3$. The diffraction peaks at 2θ angles appeared in the order of 20.79 °, 29.60 °, 42.20 °, 52.49 °, 61.42 °, 65.52 °, 69.77 ° and 77.50 ° and can be assigned to scattering from the (010), (1 1 0), (1 1 4), (0 2 0), (0 1 5), (0 1 7), (2 2 0) and (2 0 6) planes of the BaPbO$_3$ perovskite type crystal lattice, respectively. XRD data shows BaPbO$_3$ crystallized in an orthorhombic space group with
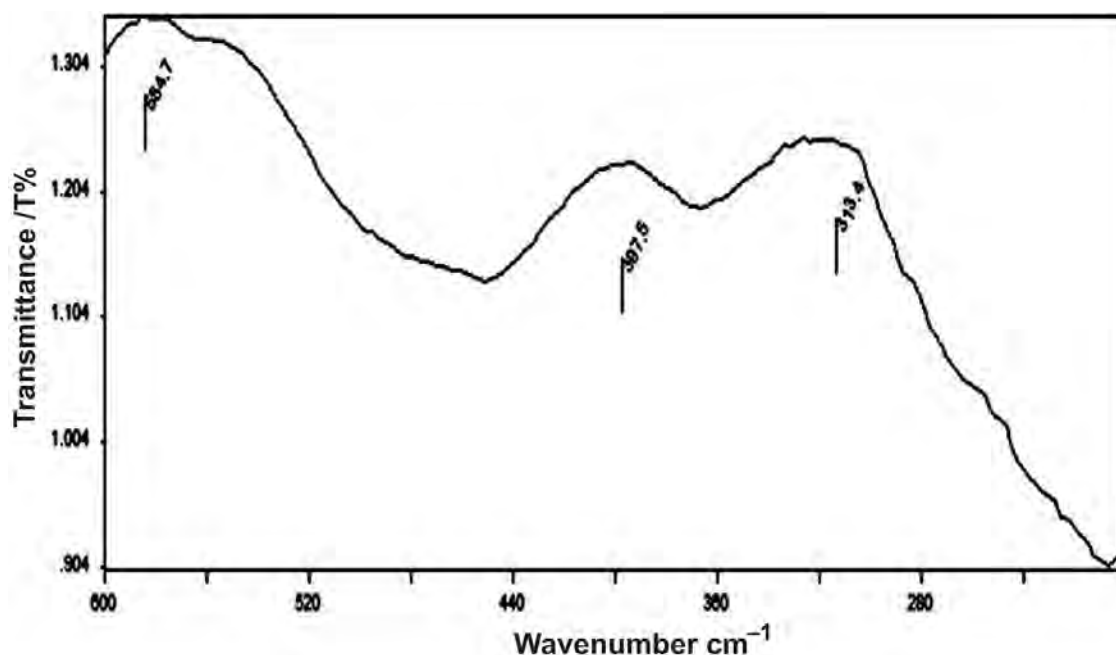

Figure 3 IR spectrum of BaPbO$_3$ calcinated at 700 °C.

a = 6.185, b = 6.152 and c = 8.639. The crystallite sizes were calculated using XRD peak broadening of the (110) peak and Scherrer's formula:

$$D_{hkl} = \frac{0.9\lambda}{\beta_{hkl}\cos\theta_{hkl}},$$

where D_{hkl} (nm) is the particle size perpendicular to the normal line of the (hkl) plane, β_{hkl} is the full width at half maximum, θ_{hkl} (Rad) is the Bragg angle of the (hkl) peak, and λ (nm) is the wavelength of the X-ray. The calculated particles size of $BaPbO_3$ nanoparticles calcined at 700 °C was about 38 nm.

3.2. IR Spectroscopy

The IR spectrum of the $BaPbO_3$ perovskite type oxide is presented in Fig. 3. This spectrum shows two strong and well-defined absorption bands, typical of ABO_3-type perovskite oxides. The modes in the spectral range from 200 to 600 cm^{-1} are due to the bending and stretching internal vibrations of octahedral oxygen and the O–Ba/Pb–O vibrations.

3.3. SEM and EDX Analysis

SEM analysis was carried out in order to determine the morphology of the sample. Figure 4 shows the micrograph of the samples. Based on the SEM images, the porosity of the surface is evident and it seems that the particles have grown with uniform size. The pores size varied from 1 to 3.0 μm. It must be mentioned that pores with large geometric dimensions are more suitable for water treatment. Also, the existence of micro-pores facilitates the sorption of hazardous chemicals to the surface. This phenomenon improved the efficiency and workability of $BaPbO_3$ as a photocatalyst.

The surface looks scaly and nearly fully covered with the particles that have grown on it. Further, it can be seen from the SEM results that, in addition to the larger particles (0.5–2 μm), the surface contains also smaller particles. However, the appearance of bigger particles on the surface seems to be dominant. The aggregation of the smaller particles (in the nm range) may result in bigger $BaPbO_3$ particles on the surface. EDX analysis was performed to confirm the composition. Figure 5 shows the EDX spectrum, which indicates the existence of Ba, Pb, and O. Quan-
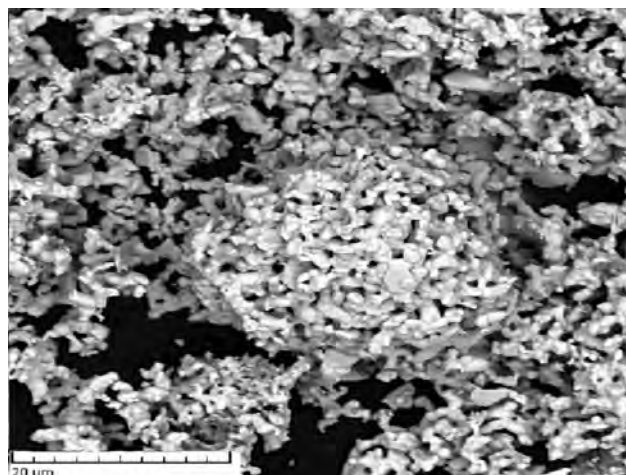

Figure 4 SEM image of $BaPbO_3$ calcinated at 700 °C.

titative analysis of the EDX data, gave Ba, Pb and O in the molar ratio of 1:1:3.

3.4. TEM Analysis

The size of the perovskite particles was evaluated and confirmed using TEM. Figure 6 shows a representative TEM image of $BaPbO_3$. The particle size is approximately 40 nm. It is clear that the perovskite nanoparticles consist of particles smaller than 50 nm. As the TEM images show, the morphology of nanoparticles is homogeneous. It can be seen that the obtained value (around 40 nm) is in agreement with the result obtained from XRD measurement.

3.5. Photocatalysis of Methylene Blue (MB)

The efficiency of the prepared and characterized $BaPbO_3$ nanoparticles as an adsorbent for the removal of MB from liquid solutions was investigated using a batch equilibrium technique. Different amounts of adsorbent were placed in a glass bottle containing 100 mL of a dye solution at 30 mg L^{-1} concentration. The adsorption studies were carried out at different pH values, catalyst concentration and hydrogen peroxide concentrations and the results are presented in the following sections.
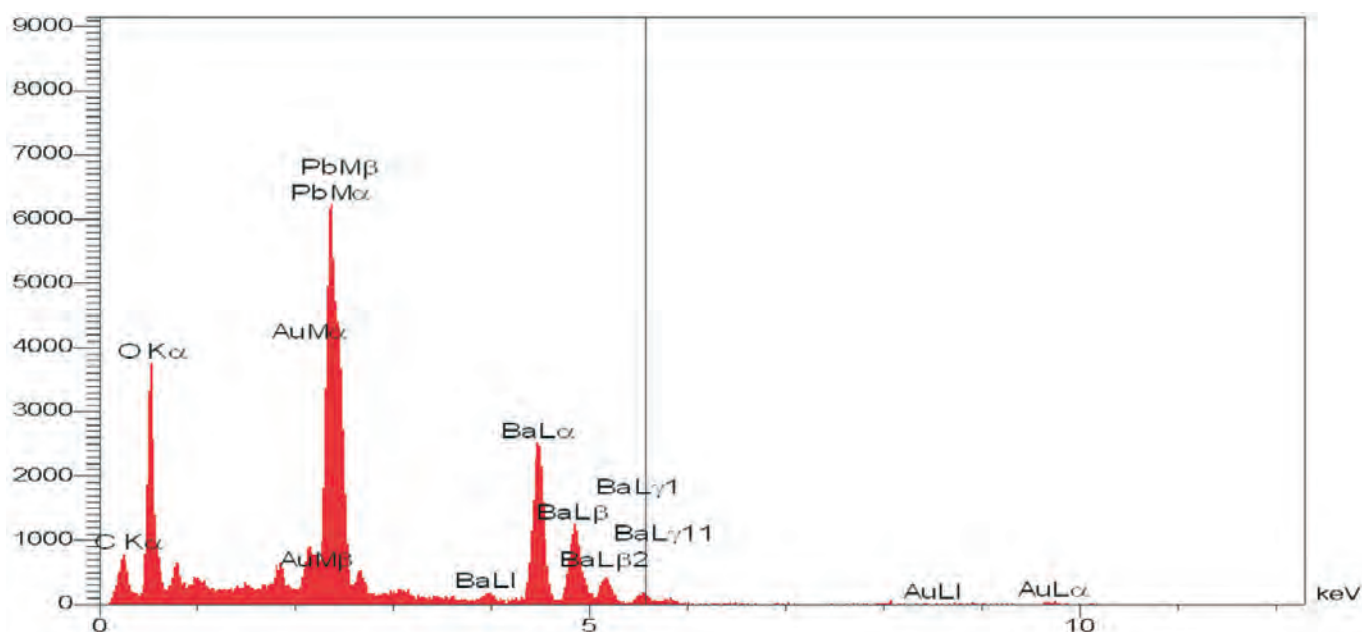

Figure 5 Energy dispersive X-ray (EDX) spectrum of the $BaPbO_3$ nanoparticles calcined at 700 °C.
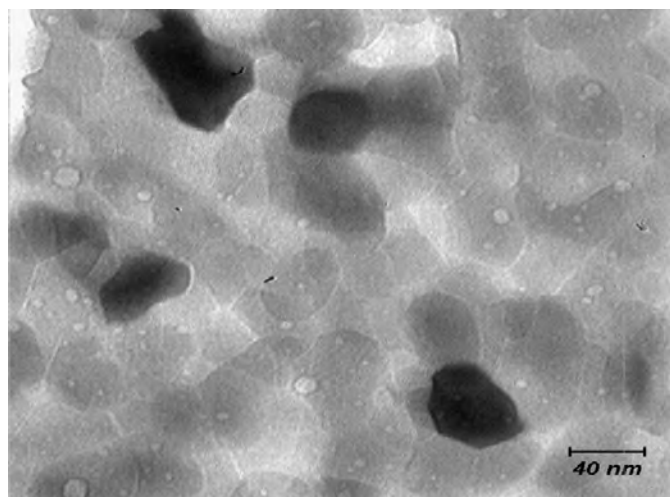
Figure 6 TEM image of $BaPbO_3$ calcined at 700 °C.

3.5.1. *Effect of Photocatalyst Concentration in Suspension*

Figure 7 shows the influence of photocatalyst concentration in suspension on MB decomposition, as a function of UV irradiation time. Extending the illumination time resulted in reduced MB content in the suspension. In general, the degradation ratio was higher than 92 % over the four different concentrations of photocatalysts after 60 min of UV irradiation. It can be also seen from Fig. 7 that increasing the powder concentration from 0.1 to 0.2 g 100 mL^{-1} lead to an enhanced degradation rate, but that there was little change in degradation rate 0.2 to 0.4 g 100 mL^{-1}. This was most probably due to stronger light reflection on the photocatalyst powder. Irrespective of the catalyst concentration, after 60 min, 99 % of the MB was oxidized. Using rutile as a photocatalyst, under the same experimental conditions, 90.4 of the MB was oxidized. In other words, the photocatalytic activity of $BaPbO_3$ is higher than the rutile phase.[19]

3.5.2. *Effect of pH*

Figure 8 shows the effect of pH on the photocatalytic activity. The initial pH varied in the range of 6-11. The photodegradation efficiency as a function of pH value decreases in the order of 11 >
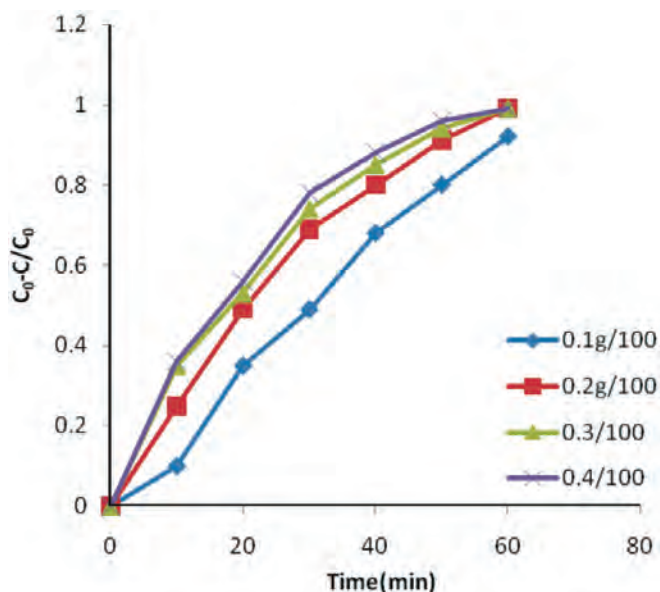

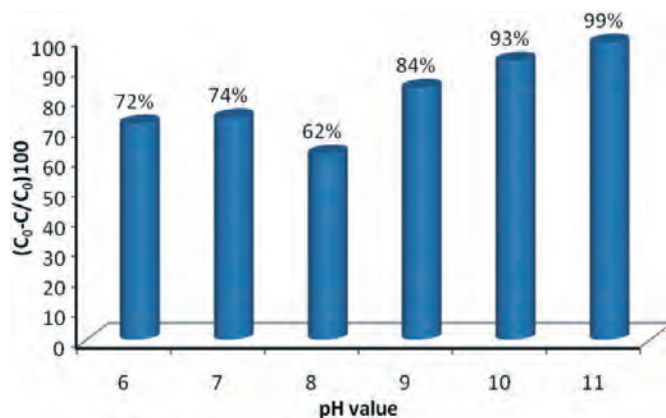**Figure 7** Dependence of MB degradation on nanopowder concentration in suspension.

Figure 8 Dependence of photocatalytic activity on pH value in suspension after 30 min UV irradiation.

10 > 9 > 6 7 > 8, where the conversion of MB at pH 11 and 6 are about 99 and 72 %, respectively. It is generally accepted that pH-dependent photodecomposition is principally attributed to variations in surface charge properties of the photocatalyst.[20] As a result, this changes the adsorption conduct of a dye on the catalyst surface. Since MB has a cationic configuration, its adsorption is preferred in alkaline solution as shown in Fig. 9. The increasing pH value results in a higher adsorption of MB on the $BaPbO_3$ surface. There is a sharp adsorption in the pH range 8 to 10. This pH region may match the point of zero charge for $BaPbO_3$. As MB decolorization under UV irradiation occurs mainly on the surface, positive pores or hydroxyl radicals may efficiently oxidize the MB in contact with the $BaPbO_3$.

As seen comparatively in Figs 8 and 9, the pH-dependent adsorption and photodegradation are in acceptable in the pH range 8 to 11. However, at a pH between 6 and 7, the results are disputable. The reason may be the production of HO_2^- oxidant in the presence of H^+, which promotes the MB oxidation over $BaPbO_3$ under weakly acidic solution.[21]

3.5.3. *Effect of H_2O_2*

The effect of H_2O_2 on the decolorization of MB was studied at different concentrations of MB. The change of dye concentration as a function of time for the initial concentration of 10 mg L^{-1} is shown in Fig. 10. Initial results in Fig. 11 also show that neither UV irradiation alone nor H_2O_2 alone was capable of decolorizing MB. Therefore, the combination of UV/H_2O_2 was necessary. Increasing the H_2O_2 concentrations from 0.2 to 4 mL L^{-1}, significantly reduced the time required to decolorize the MB solution.
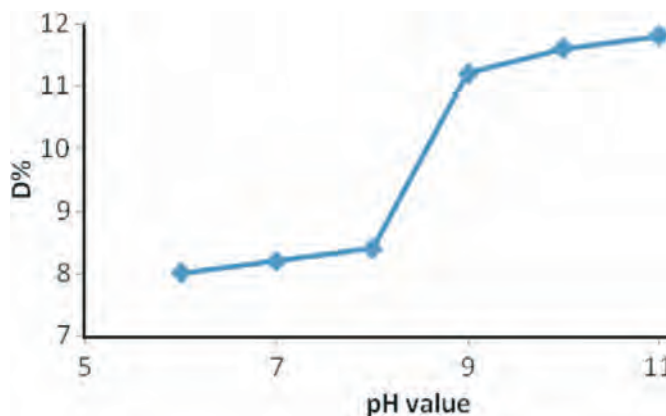

Figure 9 pH-dependent adsorption of MB on powder surface, D(%) C_0 C_e)/C_e × 100, where D is distribution ratio, C_0 means initial concentration of MB, C_e denotes equilibrium concentration.[22]
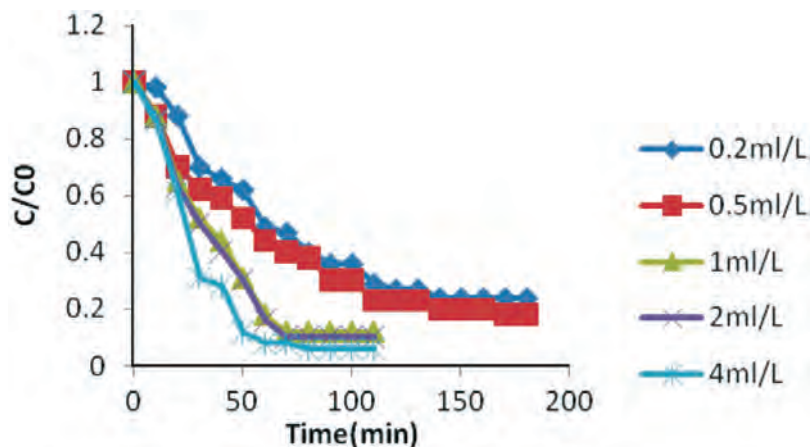
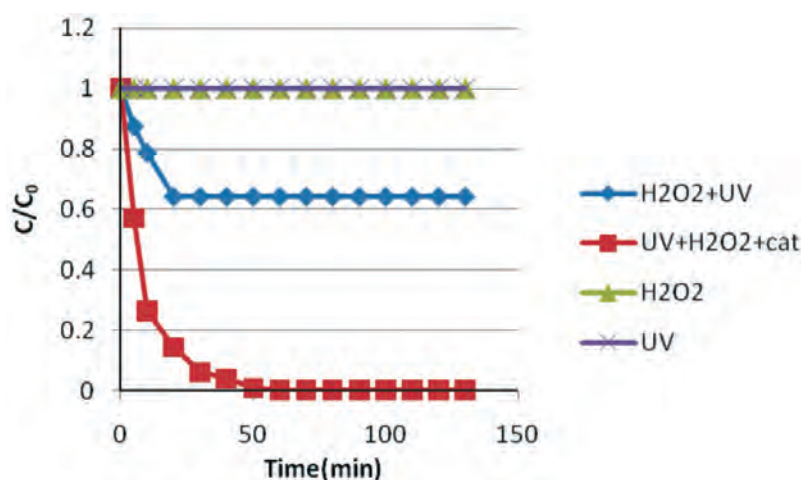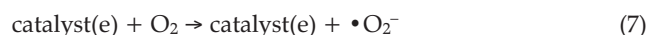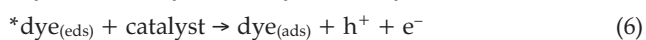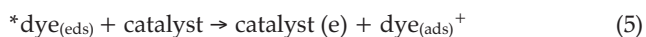**Figure 10** Decolorization of MB under different concentrations of H_2O_2.

Figure 11 Decolorization of MB under 0.2 g 100 mL^{-1} cat, 0.05 mL L^{-1} H_2O_2 and UV irradiation.

Similar behaviour was observed for 20 mg L^{-1}, 30 mg L^{-1}, 40 mg L^{-1} and 50 mg L^{-1} of dye concentration. However, at high concentrations of dye, decolorization needs higher dosages of H_2O_2. We examined the decolorization of MB using UV, H_2O_2 and BaPbO$_3$. The results revealed that the decolorization of MB under this condition occurred in less time than the UV/H_2O_2 alone. As Fig. 11 shows that when 0.1 mL L^{-1} of H_2O_2 is combined with UV light in the absence of BaPbO$_3$, photodegradation of MB is not completed. In the presence of the catalyst, however, MB photodegradation occurred completely in the suspension.

There are three possible reaction mechanisms for decolorization of MB in our experiment. The catalytic, UV photodegradation could proceed according to Equations 1–3.

$$\text{Catalyst (h)} \rightarrow h^+ + e^- \tag{1}$$

$$e^- + O_2 \rightarrow \bullet O_2 \tag{2}$$

$$h^+ + OH^- \rightarrow \text{Catalyst (h)} + \bullet OH \tag{3}$$

Alternatively, the beginning of this process could be characterized by Equations 4 to 7. The dye adsorbed on a catalyst is stimulated by UV light and then a photoinduced electron, on the dye, is transferred to the conduction band of the catalyst. Subsequently, this reacts with molecular oxygen to form the $\bullet O_2^-$ oxidant.[23]

$$\text{dye}_{(ads)} \rightarrow \text{*dye}_{(eds)} \tag{4}$$

$$\text{*dye}_{(eds)} + \text{catalyst} \rightarrow \text{catalyst (e)} + \text{dye}_{(ads)}^+ \tag{5}$$

$$\text{*dye}_{(eds)} + \text{catalyst} \rightarrow \text{dye}_{(ads)} + h^+ + e^- \tag{6}$$

$$\text{catalyst(e)} + O_2 \rightarrow \text{catalyst(e)} + \bullet O_2^- \tag{7}$$

The third mechanism for MB decomposition results from the photolysis process. Photocatalytic degradation of MB is closely related to the structure stability of the MB, the adsorption of the MB on the catalyst surface, as well as the absorbance of the MB under light irradiation.[24] In other words, factors that can reduce MB stability, increase its absorbability and intensify its light absorbance would effectively promote photodegradation efficiency. Especially, the photocatalytic process and photolysis process are mainly associated with MB's structure stability, commonly measured by the energy required for decomposing MB molecular structure, i.e. the $\lambda_{(max)}$ of MB; the photosensitization process is primarily related to MB's absorbability and light absorbance.

4. Conclusions

In summary, the sol-gel method using citric acid and subsequent calcination, was used to synthesize nano-crystalline BaPbO$_3$ powders. A study on the structural, morphological and dye-removal efficiency of these nanoparticles was performed by various analytical techniques. Powder X-ray diffraction and microscopic analysis indicated suitable crystallinity with an orthorhombic perovskite structure for the BaPbO$_3$ nanoparticles. In addition, the present investigation has shown that the synthesized BaPbO$_3$ can be a favourable surface material to remove dye from water over a wide range of dye concentrations. The processing parameters such as amount of catalyst, initial

MB concentration, pH value and H_2O_2 dosage can all affect the adsorption process meaningfully. The results show that the prepared powders could effectively remove high concentrations of MB dye molecules. Also the percentage of removal obtained in 60 minutes of stirring was 99.8 % using 0.2 g 100 mL^{-1} catalyst. In general, experimental results of the photocatalytic activity reveal that the adsorption process can achieve dye removal and $BaPbO_3$ nanocatalyst indicates suitable adsorption behaviour for the degradation of MB. However, it should be emphasized that catalytic performance under solar light leads to better results than UV irradiation or dark ambient conditions.

References

1 A.J. Esswein and D.G. Nocera, *Chem. Rev.*, 2007, 107, 4022–4047.

2 M. Anpo and M. Takeuchi, *J. Catal.*, 2007, 216, 505–516.

3 M.A. Brown and S.C. De Vito, *Crit. Rev. Environ. Sci. Technol.*, 1993, 23, 249–324.

4 R. Christie, *Colour Chemistry*, The Royal Society of Chemistry, Cambridge, United Kingdom, 2001.

5 E.N. El Qada, S.J. Allen and G.M. Walker, *Chem. Eng. J.*, 2008, 135, 174–184.

6 S. Chatterjee, D.S. Lee, M.W. Lee and S.H. Woo, *Bioresour. Technol.*, 2009, 100, 3862–3868.

7 C. Xia, Y. Jing, Y. Jia, D. Yue, J. Ma and X.Yin, *Desalination*, 2011, 265, 81–87.

8 A.L. Ahmad and S.W. Puasa, *Chem. Eng. J.*, 2007, 132, 257–265.

9 J. Labanda, J. Sabate and J. Llorens, *J. Membr. Sci.*, 2009, 340, 234–240.

10 M.E. Osugi, K. Rajeshwar, E.R.A. Ferraz, D.P. de Oliveira, R. Arojo and M.V.B. Zanoni, *Electrochim. Acta*, 2009, 54, 2086–2093.

11 M.B. Kasiri and A.R. Khataee, *Desalination*, 2011, 270, 151–159.

12 F. Yi, S. Chen and C. Yuan, *J. Hazard.Mater.*, 2008, 157, 79–87.

13 A.R. Tehrani-Bagha, N.M. Mahmoodi and F.M. Menger, *Desalination*, 2010, 260, 34–38.

14 G. Mezohegyi, F. Goncalves, J.J.M. Orfao, A. Fabregat, A. Fortuny, J. Font, C. Bengoa and F. Stuber, *Appl. Catal. B: Environ.*, 2010, 94, 179–185.

15 K.K.H. Choy, G. McKay and J.F. Porter, *Resour. Conserv. Rec.*, 1999, 27, 57–71.

16 H. Jeong, T. Kim, D. Kim and K. Kim, *Int. J. Hydrogen Energy*, 2006, 31, 1142–146.

17 M. Carbajo, F.J. Beltran, F. Medina, O. Gimeno and F.J. Rivas, *Appl. Catal. B: Environ.*, 2006, 67, 177–86.

18 M. Yazdanbakhsh, H. Tavakkoli and S.M. Hosseini, *Desalination*, 2011, 281, 388-395.

19 H. Shi, T. Zhang and H. Wang, *J. Rare Earth.*, 2011, 29, 746-752.

20 J. Zhang, H. Deng and L. Lin, *Molecules*, 2009, 14, 2747-2757.

21 O. Carp, C.L. Huisman and A. Reller, *Prog. Solid State Chem.*, 2004, 32, 33-177.

22 Y. Shiraishi, N. Saito and T. Hirai, *J. Am. Chem. Soc.*, 2005, 127, 12820-12822.

23 C. Nasr, K. Vinodgopal, L. Fisher, S. Hotchandani, A.K. Chattopadhyay, P.V. Kamat, *J.Phys. Chem.*, 1996, 100, 8436-8442.

24 W.S. Kuo, P.H. Ho, *Dyes Pigments*, 2006, 71, 212-217.